UNIVERSITY
OF TRENTO

DEPARTMENT OF INFORMATION AND COMMUNICATION TECHNOLOGY

38050 Povo – Trento (Italy), Via Sommarive 14
http://www.dit.unitn.it

MICROWAVE IMAGING FROM LIMITED-ANGLE SCATTERED DATA USING THE ITERATIVE MULTI-SCALING APPROACH

Massimo Conci, Massimo Donelli, Gabriele Franceschini, and Andrea Massa

August 2004

Technical Report DIT-04-063

Microwave Imaging from Limited-Angle Scattered Data using the Iterative Multi-Scaling Approach

Massimo Conci, Massimo Donelli, Gabriele Franceschini, and Andrea Massa

Department of Information and Communication Technologies,

University of Trento, Via Sommarive 14, 38050 Trento - Italy

Tel. +39 0461 882057, Fax +39 0461 882093, E-mail: *andrea.massa@ing.unitn.it*

Web-site: *http://www.eledia.unitn.it*

Microwave Imaging from Limited-Angle Scattered Data using the Iterative Multi-Scaling Approach

Massimo Conci, Massimo Donelli, Gabriele Franceschini, and Andrea Massa

Abstract

In this paper, with reference to limited-angle data configurations, the performance of the nonlinear multi-scaling inversion approach (IMSA) is analyzed. Such an assessment is carried out by considering synthetically-generated as well as laboratory-controlled experimental data ('*Marseille data*') concerning two-dimensional dielectric scatterers. The obtained results demonstrate a satisfactory robustness and the reliability of the approach.

Key words:

Microwave Imaging, Inverse Scattering, Experimental Data, Limited-Angle Data Configuration.

1 Introduction

The problem of reconstructing the profile of unknown targets from experimental scattered data has two main critical features. The first one, more general and common to the retrieval from synthetically-generated data, is represented by the ill-conditioning and the nonlinearity arising from multiple scattering phenomena. It remains an open problem, however a set of very interesting and effective approaches, currently under development for successive applications to real-world situations, have been proposed in the last years (see for example [1][2] and the references cited therein for a general overview). The other lies in the fact that inverse scattering methods are expected to perform well when scattering data are taken all around the target and to decrease their efficiency in correspondence with limited-angle measurements. However, in many realistic situations, a complete measurement of the observations cannot be realized. Generally, the receivers cannot be placed close to the transmitters for mechanical reasons, or due to obstacles around the scatterer, as well as in order to avoid dangerous mutual coupling effects between transmitters and receivers. We often encounter situations where the unknown object can only be accessed over a limited angle, as opposed to the case generally dealt with where it is possible to make measurements over the full measurement range (360°). This is, for example, the case of industrial processes.

In this paper, such a situation (which belongs to the class of *aspect-limited imaging* problems) is analyzed by using the iterative multi-scaling approach (IMSA). The paper is organized as follows. In Sect. 2, the IMSA is briefly recalled. Then in Sect. 3 an exhaustive assessment of the effectiveness of the method in dealing with limited-angle scattered data is presented by considering synthetic (modeling realistic scenarios) as well as experimental test cases. Finally, some conclusions are reported (Sect. 4).

2 The Iterative Multi-Scaling Approach

Let us consider the nonlinear multi-resolution inversion approach proposed in [3] for a two-dimensional scenario. At each fixed frequency, f , the two-dimensional inverse scattering problem can be mathematically described through the *data equation* and *state equation*

$$E^v_{scatt}(x_{m_{(v)}}, y_{m_{(v)}}) = \Im_{ext}\left\{\tau(x', y'),\, E^v_{tot}(x', y');\, (x', y') \in D_I\right\} \quad (x_{m_{(v)}},\, y_{m_{(v)}}) \in D_M \tag{1}$$

$$E^v_{inc}(x, y) = \Im_{int}\left\{\tau(x', y'),\, E^v_{tot}(x', y');\, (x', y') \in D_I\right\} \quad (x,\, y) \in D_I \tag{2}$$

$\Im_{ext}$ and $\Im_{int}$ being the external and internal scattering operators [4] and $v = 1, ..., V$ the index indicating different multi-illumination/multi-view positions.

The data of the problem are the incident electric field measured inside the *investigation domain* D_I, where the unknown scattering object is supposed to be located, $E^v_{inc}(\,.\,)$, and the scattered electric field, $E^v_{scatt}(\,.\,)$, collected at a set of measurement points $\left(x_{m_{(v)}},\, y_{m_{(v)}}\right)$, $m_{(v)} = 1, ..., M_{(v)},\ v = 1, ..., V$ belonging to the *observation domain* (D_M) and located outside D_I. As far as the *problem unknowns* are concerned, they are the *contrast function* $\tau(x, y)$, $(x, y) \in D_I$ and the electric field inside the investigation domain, $E^v_{tot}(x, y)$, $v = 1, ..., V$, $(x, y) \in D_I$.

To retrieve the unknown functions, addressing at the same time the ill-conditioning issue, the IMSA recasts the problem into the optimization of a multi-scaling multi-resolution function defined at each step, $s = 1, .., S_{opt}$, of the multi-scaling process as follows

$$\Phi^{(s)}\left\{\tau\left(x_{n_{(r)}}, y_{n_{(r)}}\right),\, E^v_{tot}\left(x_{n_{(r)}}, y_{n_{(r)}}\right);\, r = 1, ..., R = s;\, n_{(r)} = 1, ..., N_{(r)};\, v = 1, ..., V\right\} =$$
$$\frac{\sum_{v=1}^{V}\sum_{m_{(v)}=1}^{M_{(v)}}\left|E^v_{scatt}\left(x_{m_{(v)}}, y_{m_{(v)}}\right) - \Im_{ext}\left\{\sum_{r=1}^{R}\sum_{n_{(r)}=1}^{N_{(r)}} w\left(x_{n_{(r)}}, y_{n_{(r)}}\right)\tau\left(x_{n_{(r)}}, y_{n_{(r)}}\right)E^v_{tot}\left(x_{n_{(r)}}, y_{n_{(r)}}\right)\right\}\right|^2}{\sum_{v=1}^{V}\sum_{m_{(v)}=1}^{M_{(v)}}\left|E^v_{scatt}\left(x_{m_{(v)}}, y_{m_{(v)}}\right)\right|^2} +$$
$$\frac{\sum_{v=1}^{V}\sum_{r=1}^{R}\sum_{n_{(r)}=1}^{N_{(r)}}\left|w\left(x_{n_{(r)}}, y_{n_{(r)}}\right)E^v_{inc}\left(x_{n_{(r)}}, y_{n_{(r)}}\right) - \Im_{int}\left\{\sum_{q_{(r)}=1}^{N_{(r)}} w\left(x_{q_{(r)}}, y_{q_{(r)}}\right)\tau\left(x_{q_{(r)}}, y_{q_{(r)}}\right)E^v_{tot}\left(x_{q_{(r)}}, y_{q_{(r)}}\right)\right\}\right|^2}{\sum_{v=1}^{V}\sum_{r=1}^{R}\sum_{n_{(r)}=1}^{N_{(r)}}\left|w\left(x_{n_{(r)}}, y_{n_{(r)}}\right)E^v_{inc}\left(x_{n_{(r)}}, y_{n_{(r)}}\right)\right|^2} \tag{3}$$

where w is the weighting function

$$w\left(x_{n_{(r)}}, y_{n_{(r)}}\right) = \begin{cases} 0 & if \quad \left(x_{n_{(r)}}, y_{n_{(r)}}\right) \notin D_{(s-1)} \\ 1 & if \quad \left(x_{n_{(r)}}, y_{n_{(r)}}\right) \in D_{(s-1)} \end{cases} \tag{4}$$

allowing a synthetic zoom in the squared investigation domain, $D_{(s-1)}$, centered at

$$x_{c_{(s-1)}} = \frac{x_{re_{(s-1)}} + x_{im_{(s-1)}}}{2}, \quad y_{c_{(s-1)}} = \frac{y_{re_{(s-1)}} + y_{im_{(s-1)}}}{2} \tag{5}$$

$$x_{\Re(s-1)} = \frac{\sum_{r=1}^{R} \sum_{n_{(r)}=1}^{N_{(r)}} \left\{ x_{n_{(r)}} \Re\left[\tau\left(x_{n_{(r)}}, y_{n_{(r)}}\right)\right]\right\}}{\sum_{n_{(r)}=1}^{N_{(r)}} \left\{ \Re\left[\tau\left(x_{n_{(r)}}, y_{n_{(r)}}\right)\right]\right\}}, \quad R = s-1 \tag{6}$$

$$y_{\Re(s-1)} = \frac{\sum_{r=1}^{R} \sum_{n_{(r)}=1}^{N_{(r)}} \left\{ y_{n_{(r)}} \Re\left[\tau\left(x_{n_{(r)}}, y_{n_{(r)}}\right)\right]\right\}}{\sum_{n_{(r)}=1}^{N_{(r)}} \left\{ \Re\left[\tau\left(x_{n_{(r)}}, y_{n_{(r)}}\right)\right]\right\}} \tag{7}$$

and $L_{(s-1)}$ -sided

$$L_{(s-1)} = \frac{L_{re_{(s-1)}} + L_{im_{(s-1)}}}{2} \tag{8}$$

$$L_{\Re(s-1)} = 2 \frac{\sum_{r=1}^{R} \sum_{n_{(r)}=1}^{N_{(r)}} \left\{ \frac{\rho_{n_{(r)} c_{(s-1)}} \Re\left[\tau\left(x_{n_{(r)}}, y_{n_{(r)}}\right)\right]}{max_{n_{(r)}=1,..,N_{(r)}} \left\{ \Re\left[\tau\left(x_{n_{(r)}}, y_{n_{(r)}}\right)\right]\right\}} \right\}}{\sum_{r=1}^{R} \sum_{n_{(r)}=1}^{N_{(r)}} \left\{ \frac{\Re\left[\tau\left(x_{n_{(r)}}, y_{n_{(r)}}\right)\right]}{max_{n_{(r)}=1,..,N_{(r)}} \left\{ \Re\left[\tau\left(x_{n_{(r)}}, y_{n_{(r)}}\right)\right]\right\}} \right\}} \tag{9}$$

where $\Re$ stands for the real or the imaginary part and $\rho_{n_{(r)} c_{(s-1)}} = \sqrt{\left(x_{n_{(r)}} - x_{c_{(s-1)}}\right)^2 + \left(y_{n_{(r)}} - y_{c_{(s-1)}}\right)^2}$.

The number of discretization domains is chosen equal to the essential dimension of the scattered data [5].

The multi-resolution procedure is iterated until a "stationary condition" for the quantitative imaging of the scatterer under test is achieved ($s = S_{opt}$). Such a condition holds when

$$\eta_u^{(s)} = \left\{ \frac{\left| u_{(s+1)} - u_{(s)} \right|}{\left| u_{(s+1)} \right|} \times 100 \right\} < \eta_u \qquad u = x_c, y_c, L \tag{10}$$

where η_u, $u = x_c, y_c, L$ are fixed thresholds.

As far as the optimization method for the minimization of the cost function (3) is

concerned, since the multi-scaling method is not dependent either on the definition of the cost function or on the minimization algorithm, for simplicity, a deterministic optimizer based on the alternating direction implicit method [6] (CGADIM) is used. $\underline{\tau}_k^{(s)} = \left\{\left[\tau^{(s)}\left(x_{n_{(r)}}, y_{n_{(r)}}\right)\right]_k;\ r = 1, ..., R = s;\ n_{(r)} = 1, ..., N_{(r)}\right\}$ and $\underline{E}_k^{(s)} = \left\{\left[E_{tot}^{v\,(s)}\left(x_{n_{(r)}}, y_{n_{(r)}}\right)\right]_k;\right.$ $\left. r = 1, ..., R = s;\ n_{(r)} = 1, ..., N_{(r)};\ v = 1, ..., V\right\}$ are iteratively reconstructed (k being the iteration number) by alternatively updating the two sequences. At each step of the multi-scaling procedure, the minimization algorithm is stopped when a maximum number of iterations, K (i.e., $k \leq K$), or a threshold for the cost function value, ζ (i.e., $\Phi^{(s)}\left\{\underline{\tau}_k^{(s)}, \underline{E}_k^{(s)}\right\} \leq \zeta$), or the value of the cost function remains unaltered during a fixed percentage of the total amount of minimization-algorithm iterations (i.e., $\frac{\left|K_w \Phi^{(s)}\left\{\underline{\tau}_k^{(s)}, \underline{E}_k^{(s)}\right\} - \sum_{h=1}^{K_w}\left[\Phi^{(s)}\left\{\underline{\tau}_h^{(s)}, \underline{E}_h^{(s)}\right\}\right]\right|}{\Phi^{(s)}\left\{\underline{\tau}_k^{(s)}, \underline{E}_k^{(s)}\right\}} \leq \xi$, K_w being an integer number).

3 Reconstruction from Limited-Angle Scattered Data

In this section, a set of representative results will be reported to show the effectiveness of the proposed approach in dealing with limited-angle scattered data. Two different test cases will be presented. The one related to synthetically-generated data computed according to a standard numerical procedure and avoiding the "inverse crime" problem [7] (since different discretizations are chosen for the forward solver used to generate the data and during the inversion procedure). The other considers scattered field measured in a controlled environment [8]. In both cases, the numerical analysis has been carried out by considering a variable blind angle θ (Fig. 1) ranging from a reference configuration $\theta = \theta_{min}$ (for the synthetic data-set $\theta_{min} = 0°$ - *full-data configuration*) to a strongly limited-angle setup $\theta = 240$ according to the following rule of variation $\theta = \theta_{min} + t\Delta\theta$, $\Delta\theta = 20°$, $t = 0, ..., T_{max} = 12$.

To mathematically evaluate the performances of the approach in facing different measurement conditions, two sets of error figures are then defined. The first class of errors gives an indication on the *qualitative imaging* of the scenario under test. They are the

localization error ρ

$$\rho = \frac{\sqrt{\left[x_c^{(S_{opt})} - x_c^{ref}\right]^2 + \left[y_c^{(S_{opt})} - y_c^{ref}\right]^2}}{\lambda_0} \tag{11}$$

and the dimensional error δ

$$\delta = \left\{ \frac{L^{(S_{opt})} - L^{ref}}{L^{ref}} \right\} \times 100 \tag{12}$$

where the super-script ^{ref} indicates the reference value.

On the other hand, the reconstruction errors, defined as follows

$$\varepsilon_j = \sum_{r=1}^{R} \frac{1}{N_{(r)}^{(j)}} \sum_{n_{(r)}=1}^{N_{(r)}^{(j)}} \left\{ \frac{\tau(x_{n_{(r)}}, y_{n_{(r)}}) - \tau^{ref}(x_{n_{(r)}}, y_{n_{(r)}})}{\tau^{ref}(x_{n_{(r)}}, y_{n_{(r)}})} \right\} \times 100 \qquad R = S_{opt} \tag{13}$$

where $N_{(r)}^{(j)}$ can range over the whole investigation domain ($j \Rightarrow tot$, int, ext), measures the quality of the *quantitative imaging*.

Concerning the parametric configuration of the IMSA, the calibration parameters have been heuristically chosen and the reference values turned out to be: $\eta_{x_c} = \eta_{y_c} = 2\,\%$, $\eta_L = 5\,\%$. As far as the parameters for the optimization algorithm are concerned, their optimal values are equal to $K = 2000$, $\zeta = 10^{-4}$, $K_w = 100$, and $\xi = 10^{-2}$.

3.1 Testing against Synthetic Data

As a first example, let us consider the case of an off-centered square homogeneous dielectric ($\tau(x,\, y) = 0.5$) cylinder $L^{ref} = 0.8\,\lambda_0$ in diameter, located at $x_c = -y_c = 0.24\,\lambda_0$ in an investigation domain $2.4 \times 2.4\,\lambda_0^2$ (Fig. 2(a)). The measurement domain D_M is a complete circle ($\theta_{min} = 0°$) $1.8\,\lambda_0$ in radius partitioned into equally-spaced arcs whose mid-points serve as locations of the receivers. The number of the receivers is equal to

$$M_{(v)} = M_{max} - t, \quad t = 0, ..., T_{max}, \quad M_{max} = 21 \tag{14}$$

Starting from the free-space configuration ($\underline{\tau}_k^{(s)}\Big|_{s=k=0} = \underline{0}$, $\underline{E}_k^{(s)}\Big|_{s=k=0} = \underline{E}_{inc}^{(v)}$), the IMSA has been able to achieve the reconstructions shown in Fig. 2. As expected, from the

full-data configuration ($t = 0$ - Fig. $2(b)$) to the more complex scenario ($t = T_{max}$ - Fig. $2(d)$), the increment of θ leads to a reduction of the reconstruction accuracy as confirmed by the values of the error figures reported in Tab. I, which indicated a greater difficulty of the retrieval process in eliminating the artifacts and cleaning the external background ($\varepsilon_{ext}\rfloor_{\theta=0^\circ} = 9.8 \times 10^{-5}$ versus $\varepsilon_{ext}\rfloor_{\theta=240^\circ} = 2.2 \times 10^{-2}$). However, it should be pointed out that the reconstructed profiles share a lot of features with the reference object. Moreover, the localization is performed with a satisfactory accuracy ($\rho\rfloor_{\theta=240^\circ} = 6.7 \times 10^{-3}$) in the worst case ($\theta = 240^\circ$), too.

To model realistic situations by simulating the environmental noise, a gaussian noise, characterized by a fixed signal-to-noise ratio (SNR), has been added to synthetic data. In such a situation, concerning the *qualitative imaging* of the investigation domain, the method keeps its good reconstruction properties and a stable behavior when $SNR \geq 15\,dB$. Otherwise, as can be observed in Fig. $3(a)$, the localization effectiveness significantly changes and linearly increases in correspondence with a reduction of the measurement angle. As far as the *quantitative reconstruction* is concerned (Fig. 4), similar conclusions as for the qualitative retrieval can be drawn. Starting from $\theta = 80^\circ$, no-negligible changes occur in the reconstruction errors and such an increasing turns out to be larger when the noise level grows. As an example, the internal error ε_{int} (Fig. $4(b)$) varies between $\varepsilon_{int}]_{\theta=80^\circ}^{SNR=\infty} = 12.73$ and $\varepsilon_{int}]_{\theta=240^\circ}^{SNR=\infty} = 20.40$ in a noiseless scenario while larger variations arise when scattering data are corrupted ($\varepsilon_{int}]_{\theta=80^\circ}^{SNR=10} = 14.03$ and $\varepsilon_{int}]_{\theta=240^\circ}^{SNR=10} = 32.40$, $\varepsilon_{int}]_{\theta=80^\circ}^{SNR=5} = 17.80$ and $\varepsilon_{int}]_{\theta=240^\circ}^{SNR=5} = 39.10$).

3.2 Testing against Experimental Data

In the second experiment, the effectiveness of the IMSA in dealing with limited-angle data has been tested by using the real dataset provided by the Institut Fresnel, Marseille (France) [8]. The reference measurement setup is characterized by $M_{max} = 49$ receivers placed on a circle $760\,mm$ in radius and, due to the configuration of the devices, there exists a blind zone of $\theta_{min} = 120^\circ$. The scenario under test is illuminated by $V =$

36 different time-harmonic incident waves radiated by a horn antenna moved along a circle $720\,mm$ in radius between $\phi = 0°$ and $\phi = 350°$ in $\Delta\phi = 10°$ increments. In particular, the considered data ("dielTM_dec8f.exp") are related to a single dielectric cylinder characterized by an object function $\tau\,(x, y) = 2.0 \pm 0.3$ with circular cross-section $a = 15\,mm$ in radius and placed about $30\,mm$ from the center of the experimental setup. In order to perform the reconstruction, the IMSA has been applied to a monochromatic dataset at $f = 6\,GHz$ ($\frac{L^{ref}}{\lambda_0} = 0.6$, $\frac{x_c^{ref}}{\lambda_0} = 0$, and $\frac{y_c^{ref}}{\lambda_0} = -0.6\lambda_0$). The investigation domain is a square area of $L_{DI} = 6.0\,\lambda_0$-sided. Moreover, since the state equation (2) is based on the knowledge of the incident field and the design of the set-up does not provide such an information (but only the field in absence of the target measured on the observation domain), transmitting antennas have been approximated by line sources parallel to the cylindrical scatterer. Concerning the iterative process, the free-space configuration has been assumed as initial trial solution.

Figure 5 shows some representative examples of the reconstructions performed in correspondence with different limited-angle scenarios. The reconstruction accuracy reduces when the number of collectable data diminishes and the localization of the actual scatterer turns out to be more difficult ($\rho\rfloor_{\theta=120°} = 6.8 \times 10^{-2}$ versus $\rho\rfloor_{\theta=240°} = 5.9 \times 10^{-1}$). As expected, when only forward measures are used ($\theta > 160°$), the method is not able to understand that the position of the cylinder is off-centered and it looks for a centered object by over-estimating the actual dimension of the scatterer ($\delta\rfloor_{\theta=120°} = 9.19$ versus $\delta\rfloor_{\theta=240°} = 121.80$).

4 Conclusions

In the framework of a general assessment of the IMSA, the performances of the approach have been further evaluated by considering limited-angle data configurations. The dependence of the reconstruction on the extension of the blind area has been analyzed by considering synthetic as well as experimental test cases. The obtained results confirmed

the effectiveness of the multi-scaling procedure in such a situation, too.
However, further researches are needed to further improve the quantitative imaging. Towards this end, some studies will be devoted to fully exploit the capability of the approach in taking into account the *a-priori* information on the scenario under test as well as on the measurement setup (e.g., symmetry or asymmetry of the observation domain, features of the mechanical acquisition system).

Acknowledgments

The experimental data used herein are by courtesy of Dr. K. Belkebir and Dr. M. Saillard (Institut Fresnel, Marseille, France). The authors wish to express their gratitude to E. Vico for suggestions and discussions on the paper and Ing. Ch. Marzadro for providing some numerical results of computer simulations.

References

[1] J. Ch. Bolomey. *Frontiers in Industrial Process Tomography.* Engineering Foundation, 1995.

[2] J. Ch. Bolomey, "Microwave imaging techniques for NDT and NDE," *Proc. Training Workshop on Advanced Microwave NDT/NDE Techniques*, Supelec/CNRS, Paris, Sept. 7-9, 1999.

[3] S Caorsi, M. Donelli, D. Franceschini, and A. Massa, "An iterative multi-resolution approach for microwave imaging applications," *Microwave Optical Technol. Lett.*, vol. 32, pp. 352-356, 2002.

[4] D. S. Jones, *The Theory of Electromagnetism*. Oxford, U.K.: Pergamon Press, 1964.

[5] O. M. Bucci and G. Franceschetti, "On the degrees of freedom of scattered fields," *IEEE Trans. Antennas Propagat.*, vol. 37, pp. 918-926, 1989.

[6] R. V. Kohn and A. McKenney, "Numerical implementation of a variational method for electrical impedance tomography," *Inverse Problems*, vol. 6, pp. 389-414, 1990.

[7] D. Colton and R. Kress, *Inverse Acoustic and Electromagnetic Scattering Theory*. Springer, Berlin, 1992.

[8] K. Belkebir and M. Saillard, Special section: "Testing Inversion Algorithms against Experimental Data," *Inverse Problems*, vol. 17, pp. 1565-1702, 2001.

FIGURE CAPTIONS

- Figure 1.

  Problem geometry.

- Figure 2.

  Original profile (a). Reconstructed profile (noiseless conditions) when: (b) $\theta = 0°$, (c) $\theta = 120°$, and (d) $\theta = 240°$.

- Figure 3.

  Qualitative error figures versus blind-angle value θ for different signal-to-noise ratio SNR: (a) localization error ρ and (b) dimensional error δ.

- Figure 4.

  Quantitative error figures versus blind-angle value θ for different signal-to-noise ratios SNRs: (a) total reconstruction error ε_{tot}, (b) internal reconstruction error ε_{int}, and (c) external reconstruction error ε_{ext}.

- Figure 5.

  Experimental Validation - Reconstruction of an off-centered homogeneous circular cylinder (Real dataset "Marseille" [8] - "dielTM_dec8f.exp" - $f = 6\,GHz$): (a) $\theta = 120°$, (b) $\theta = 160°$, (c) $\theta = 200°$, and (b) $\theta = 240°$.

TABLE CAPTIONS

- Table I.

  Testing against synthetic data - Reconstruction of an off-centered homogeneous dielectric cylinder (Noiseless Conditions) - Error Figures.

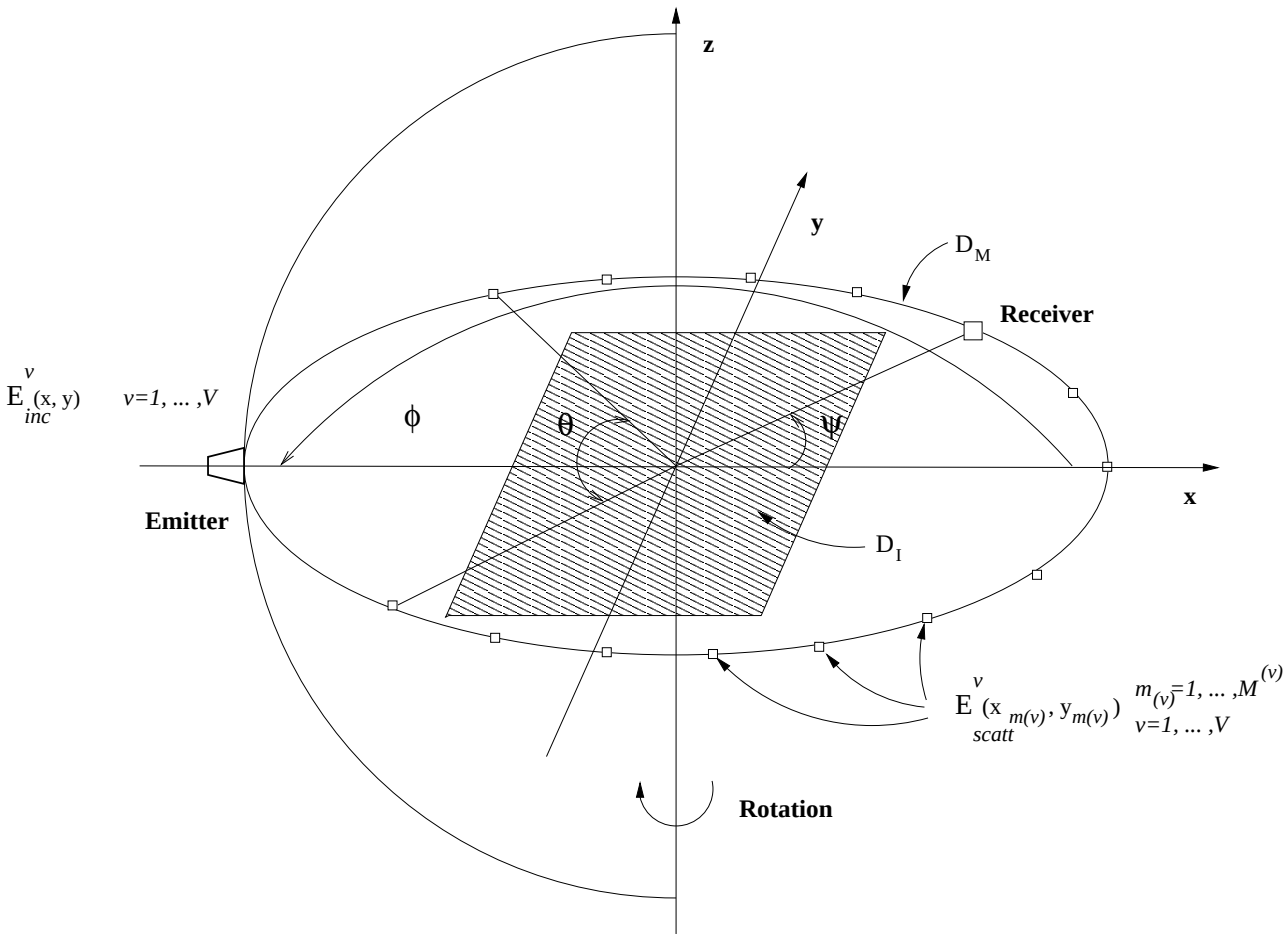

Fig. 1 - M. Conci *et al.*, "Microwave Imaging from Limited-Angle ..."

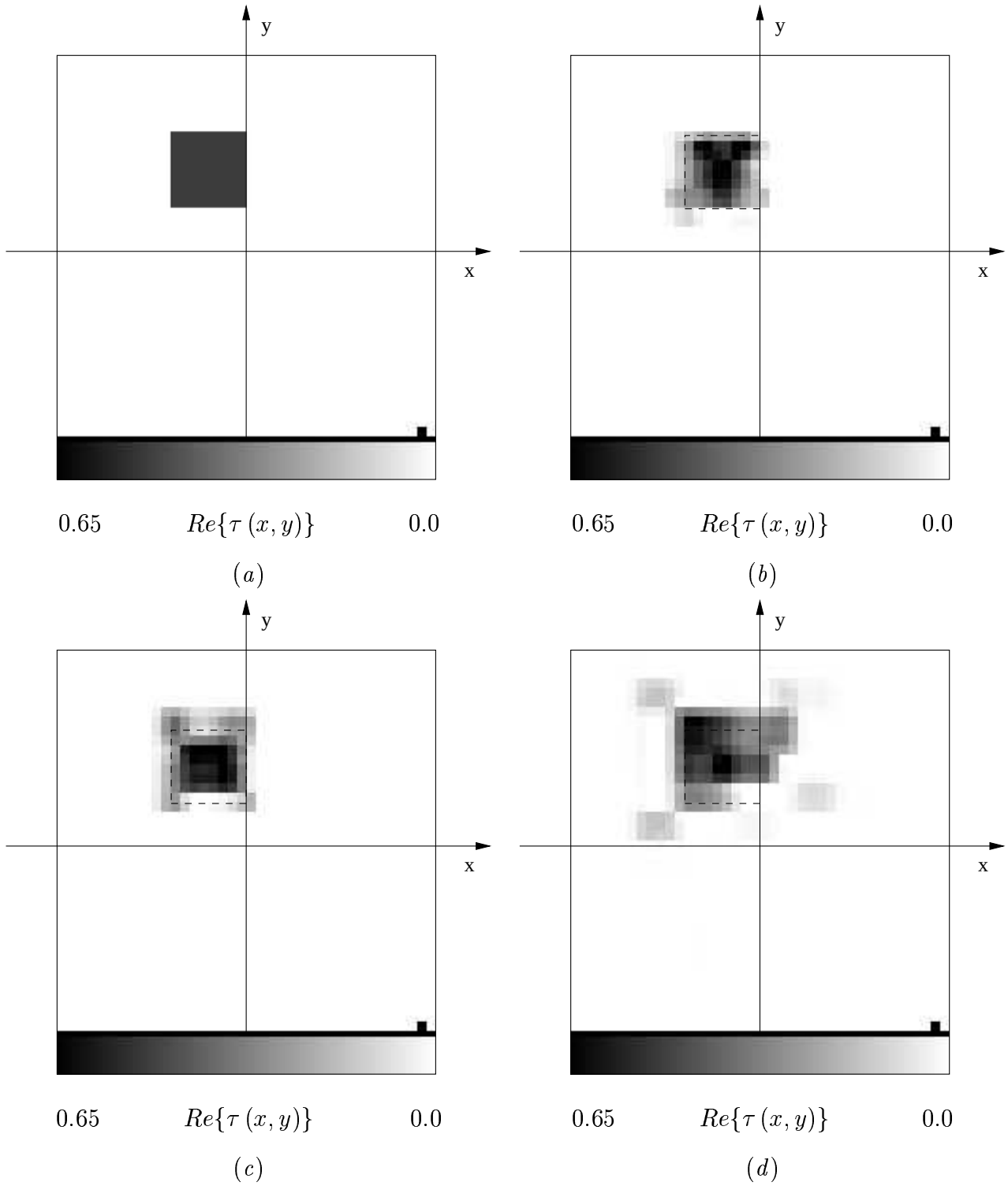

Fig. 2 - M. Conci *et al.*, "Microwave Imaging from Limited-Angle ..."

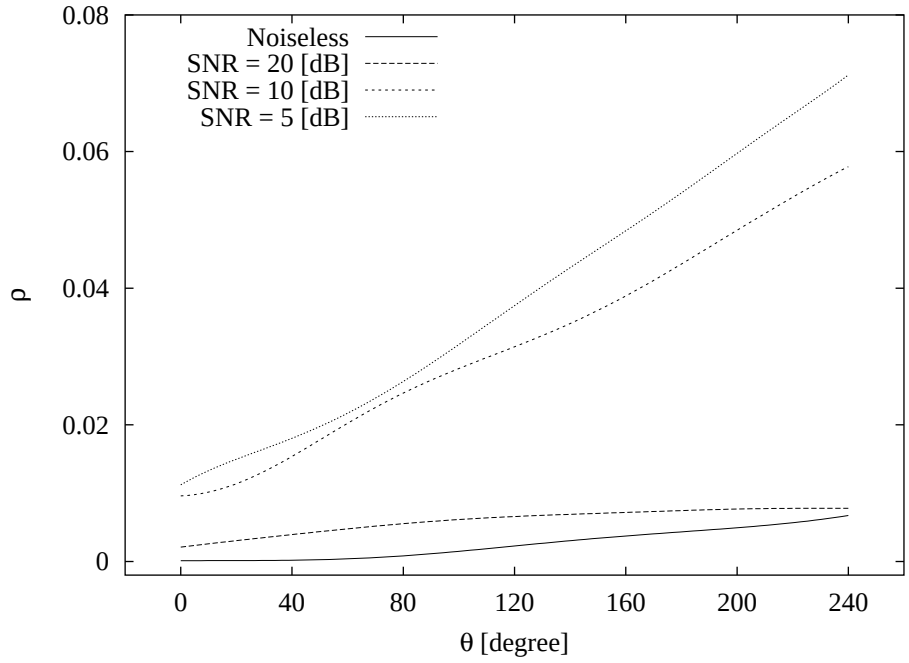

(a)

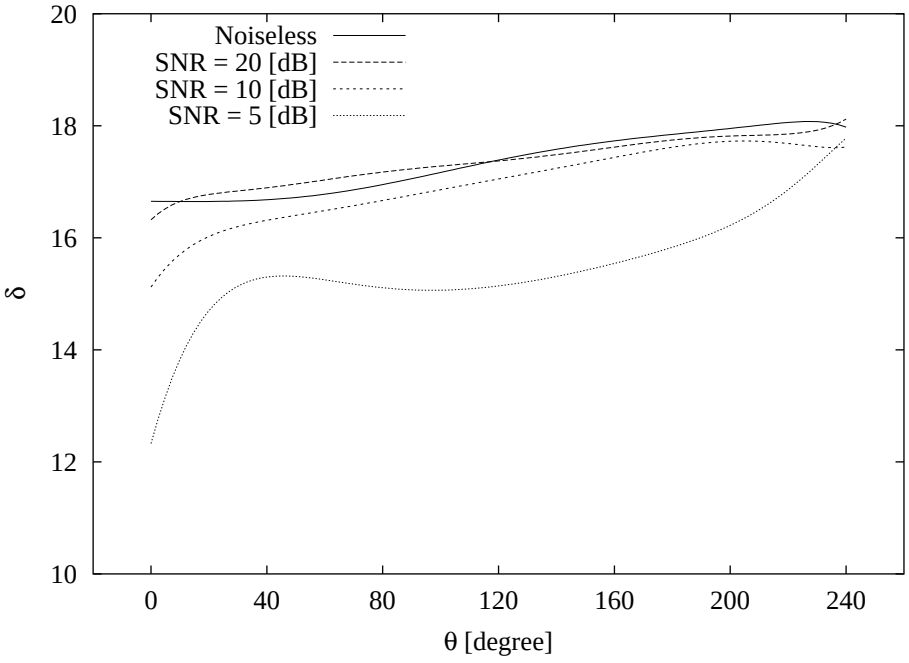

(b)

Fig. 3 - M. Conci *et al.*, "Microwave Imaging from Limited-Angle ..."

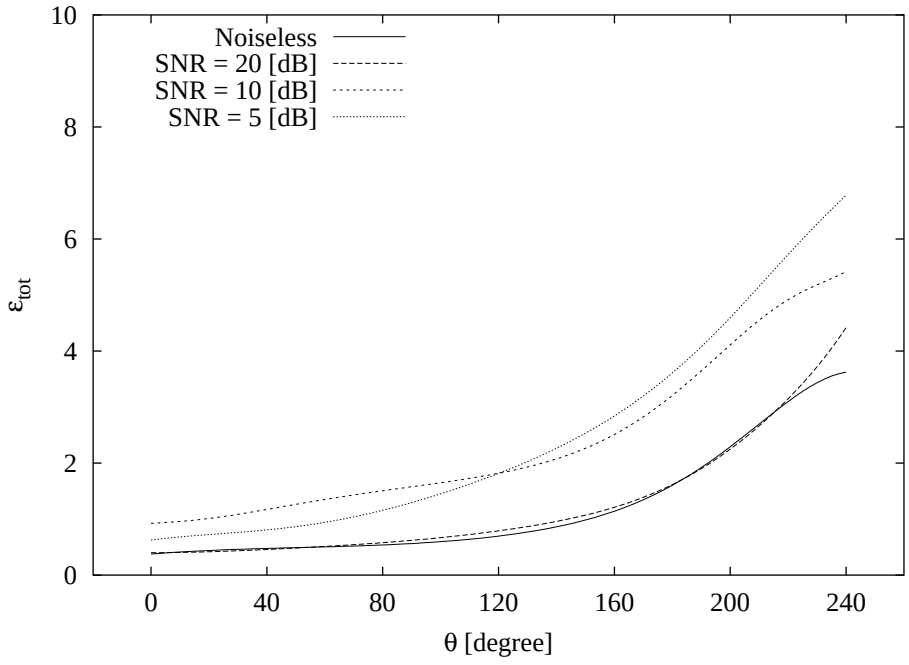

(a)

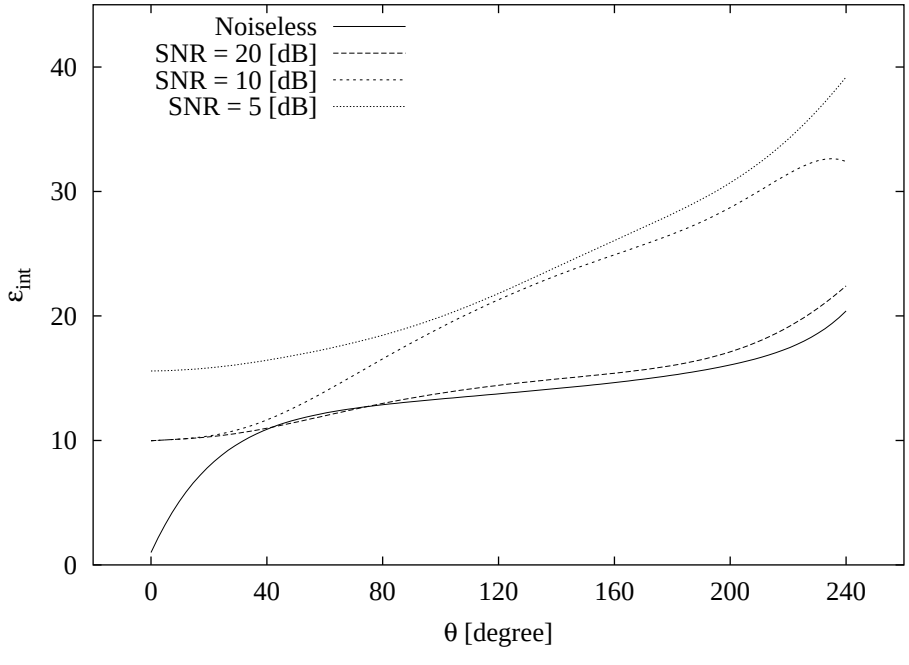

(b)

Fig. 4(I) - M. Conci *et al.*, "Microwave Imaging from Limited-Angle ..."

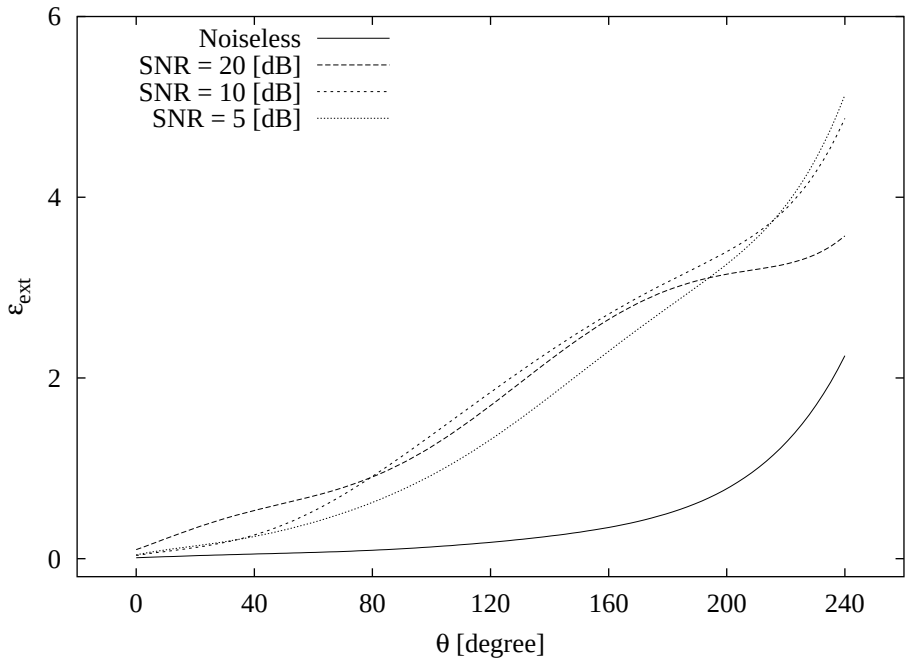

(c)

Fig. 4(*II*) - M. Conci *et al.*, "Microwave Imaging from Limited-Angle ..."

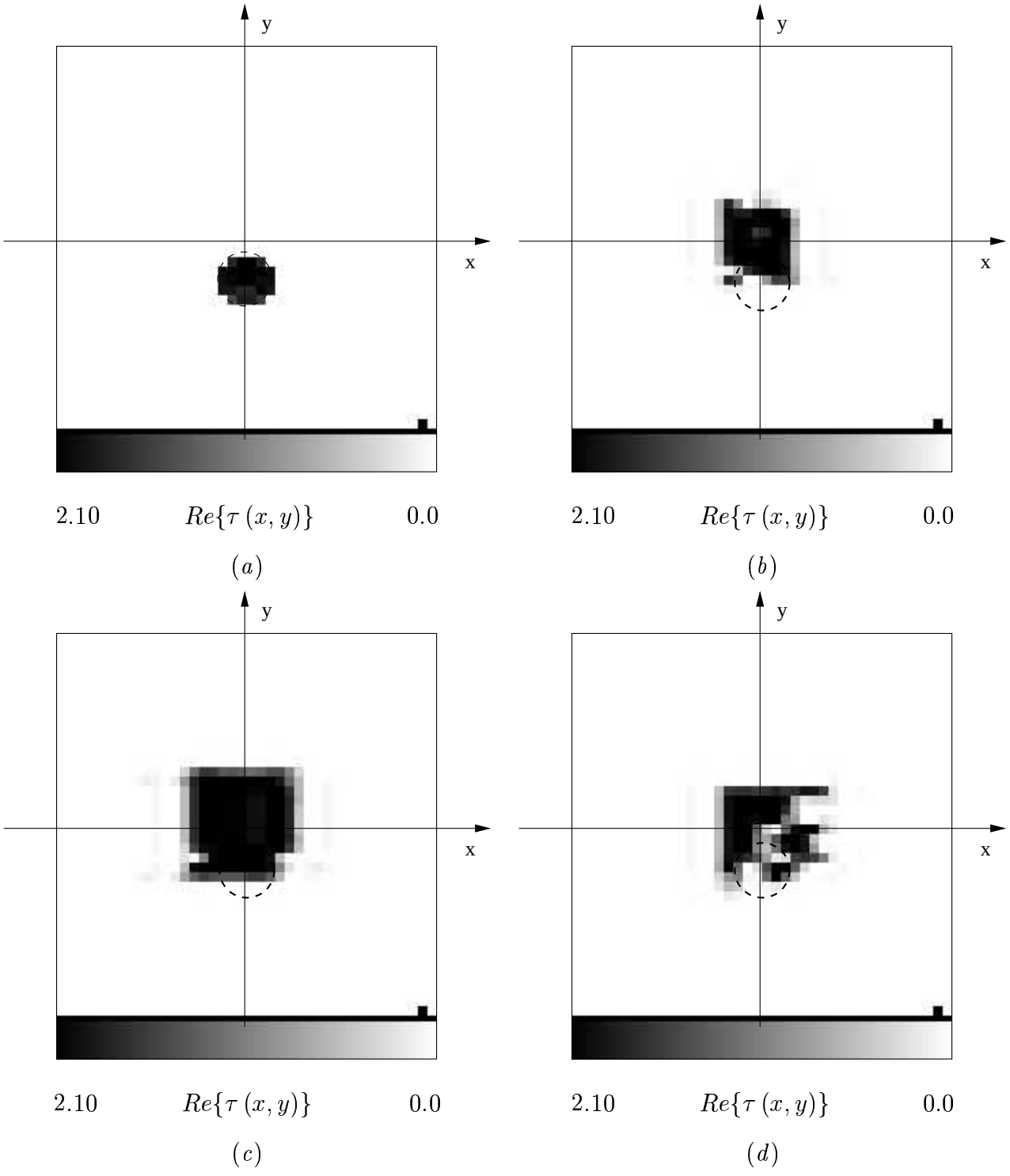

Fig. 5 - M. Conci *et al.*, "Microwave Imaging from Limited-Angle ..."

θ [deg]	ε_{tot}	ε_{int}	ε_{ext}	ρ	δ
0	0.37	0.99	9.8×10^{-5}	1.1×10^{-4}	15.12
20	0.45	11.21	3.1×10^{-4}	1.2×10^{-4}	16.68
40	0.49	12.21	6.4×10^{-4}	1.2×10^{-4}	16.23
60	0.50	12.69	6.5×10^{-4}	1.6×10^{-4}	16.29
80	0.50	12.73	7.5×10^{-4}	1.7×10^{-4}	16.29
100	0.54	13.53	7.0×10^{-4}	9.9×10^{-4}	17.16
120	0.54	13.70	1.8×10^{-3}	2.7×10^{-3}	17.19
140	0.85	13.99	2.3×10^{-3}	3.2×10^{-3}	17.31
160	0.87	14.74	2.8×10^{-3}	3.9×10^{-3}	17.66
180	0.94	14.54	3.5×10^{-3}	4.3×10^{-3}	18.18
200	2.23	16.41	5.6×10^{-3}	4.7×10^{-3}	18.23
220	3.45	15.70	9.3×10^{-3}	5.4×10^{-3}	17.50
240	3.62	20.40	2.2×10^{-2}	6.7×10^{-3}	17.61

Tab. I - M. Conci *et al.*, "Microwave Imaging from Limited-Angle ..."